ARTICLE

Check for updates

High-throughput exploration of halide perovskite compositionally-graded films and degradation mechanisms

Shahram Moradi[1,5], Soumya Kundu[2,5], Milad Rezazadeh[3], Vishal Yeddu[2], Oleksandr Voznyy [3] & Makhsud I. Saidaminov [1,2,4 ✉]

The conventional approach to search for new materials is to synthesize a limited number of candidates. However, this approach might delay or prevent the discovery of better-performing materials due to the narrow composition space explored. Here, we fabricate binary alloy films with a composition gradient in a single shot in less than one minute. We apply this approach to study the stability of halide perovskites. We synthesize all possible binary compositions from $MAPbI_3$ and $MAPbBr_3$ and then study their optical properties, structure, and environmental stability in a high-throughput manner. We find that perovskite alloys experience three different degradation mechanisms depending on halogen content: bromine-rich perovskites degrade by hydration, iodine-rich perovskites by the loss of the organic component, and all other intermediate alloys by phase segregation. The proposed method offers an avenue for discovering new materials and processing parameters for a wide range of applications that rely on compositional engineering.

[1] Department of Electrical & Computer Engineering, University of Victoria, 3800 Finnerty Rd, Victoria V8P 5C2 BC, Canada. [2] Department of Chemistry, University of Victoria, 3800 Finnerty Rd, Victoria V8P 5C2 BC, Canada. [3] Department of Physical and Environmental Sciences, University of Toronto Scarborough, Scarborough M1C 1A4 ON, Canada. [4] Centre for Advanced Materials and Related Technologies (CAMTEC), University of Victoria, 3800 Finnerty Rd, Victoria V8P 5C2 BC, Canada. [5] These authors contributed equally: Shahram Moradi, Soumya Kundu. ✉email: msaidaminov@uvic.ca

Novel material compositions are always sought after to achieve new benchmarks in photovoltaics[1,2], thermoelectrics[3], piezoelectrics[4], catalysis[5], batteries[6], superconductors[7], magnetism[8], pharmaceuticals[9], lasers, light-emission-diods[10], and other fields. Materials science has hitherto mainly relied on a "trial-and-error" approach that led to many important—but primarily serendipitous—discoveries of new materials or processing parameters[11]. For instance, NiTi shape memory alloy is one example of serendipitous discovery[12]. A more recent example is the discovery of a noble metal-free nanoparticulate electrocatalyst, CrMnFeCoNi, with catalytic activity for the oxygen reduction reaction[13]. Given that the number of potential compounds rises exponentially in multi-atom mixtures, there is a need for a more efficient and systematic search for new materials[14–21].

High-throughput methods[22,23] are developed to accelerate the discovery of materials by searching through ever-increasing vast space of multi-atom compositions[24]. In addition, high-throughput approaches provide access to big data that is now being used to train machine-learning algorithms[25], which predict and sometimes make new materials[26]. In both high-throughput and machine-learning-assisted search, the output heavily relies on the number of available data sets[27,28]. Figure 1a depicts a common strategy in conventional high-throughput methods for compositional engineering[29], when several compositions are combinatorially prepared and studied. However, this 'fragmented approach' provides discrete data sets[30], which, unfortunately, misses most of the compositions in between to form a complete experimental data set. Therefore, there is a significant need for a comprehensive method of fabrication of multinary phases to search for new compositions in a systematic manner[31–35].

Here we show an approach for a synthesis of all possible phases in binary systems in one shot. We achieve this by developing a strategy for the fabrication of compositionally-graded films (CGFs), where the film starts with one composition and gradually transitions to another through alloying. We apply our strategy to study a binary system of MAPbI$_3$ and MAPbBr$_3$ perovskites, a promising and fast-growing class of semiconductors for optoelectronics. In particular, perovskite solar cells' recently achieved 25.7% power conversion efficiency[36] in large is due to compositional engineering. Using our method, we prepare hundreds of perovskite alloys in <1 min, then study their optical and structural stability in a high-throughput manner and report compositionally stable alloy regions.

Results and discussion

We chose a slot-die coating method to fabricate CGFs. This method is promising for roll-to-roll fabrication and commercialization of solution-processed materials, including polymer and perovskite solar cells and light-emitting diodes[17,32,33,37]. Therefore, using slot-die coating will allow simultaneous optimization of processing parameters to develop device-integrable thin films.

The slot-die coating method uses a pump to supply a solution to a slot-die head that prints material on a substrate. We added a second pump and connected the outputs of the two solution supplies (Fig. 1b) using a unidirectional Y junction. The liquid mixture then flows into a slot-die head reservoir where it experiences a sudden change in cross-section area and shape (from circular to truncated cylinder), leading to proper mixing[38].

We first programmed one pump to decrease its solution supply gradually while the other pump—to increase it. However, this approach led to nonlinear and discontinuous gradient films due to the delayed arrival of second ink as it starts at a low speed. We then alternated ink supply using the slot-die coating profile depicted in Supplementary Fig. 1. After filling the slot-die head with one ink, we stopped its supply and started supplying the second ink at high speed, simultaneously moving the slot-die along the substrate. This alternated ink supply approach allowed for in situ mixing of two solutions and in situ gradient change of final solution composition and enabled the fabrication of CGFs, as we show below.

Figure 2a, b shows top- and side-views of CGF prepared from MAPbBr$_3$ and MAPbI$_3$ solutions on a 28 cm long substrate fabricated within <1 min. The visual appearance of the film, i.e., continuous yellow to black transition through the film, indicates that the film is made of MAPbBr$_3$ and MAPbI$_3$ at $l = 0$ and $l = 28$ cm, respectively, and all possible MAPb(I$_x$Br$_{1-x}$)$_3$ alloys while moving through the length of the film from one side to another.

To validate the gradient nature of the CGF, we measured the absorption bandgap along the center of the film. We used a robotic arm to slide a spectrometer's reflection probe to measure CGF's optical property in equally-spaced 215 locations along the center of the film (Supplementary Fig. 2 and Supplementary Movie 1). We then processed the data using MATLAB code (Supplementary Data 1) to compute the Tauc plot and the bandgaps (Fig. 2d, e). The bandgaps of the CGF indeed gradually decrease from 2.23 to 1.62 eV while moving from $l = 0$ to
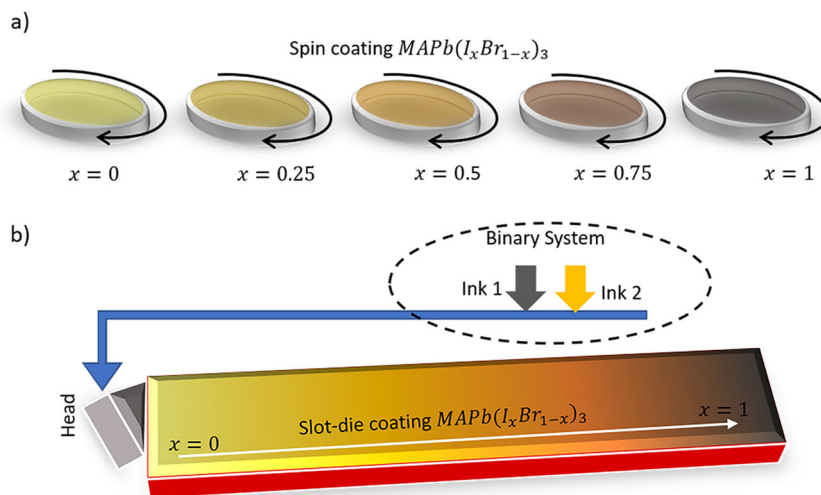

Fig. 1 Schematic of approaches for material composition optimization. a Conventional approach to fabricate a limited number of compositions. **b** Fabrication of compositionally-graded films (CGFs) that include all possible phases from binary systems in one shot.
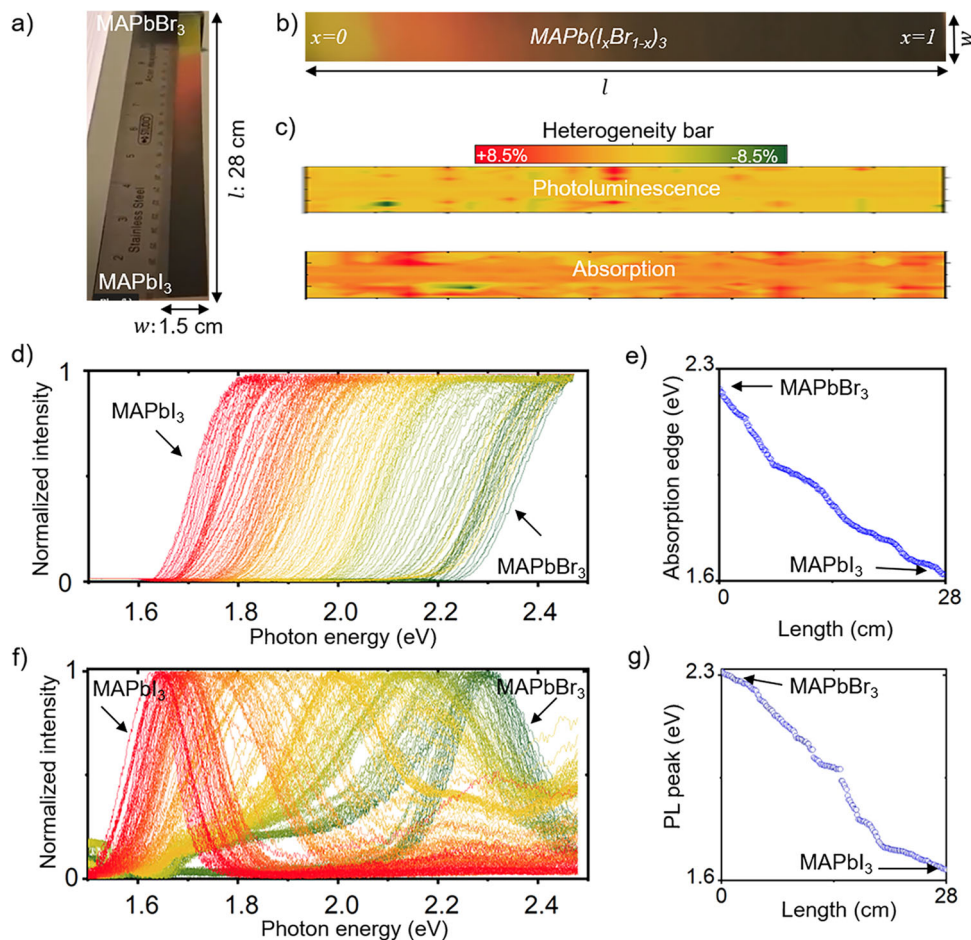
Fig. 2 Characterization of CGFs. a Side-view and **b** top-view of CGF. **c** Quantification of heterogeneity across the width of the CGF by normalizing absorption and photoluminescence bandgaps to the center of the CGF. **d** Normalized absorption Tauc plots of fresh CGF and **e** extracted absorption bandgaps for 215 locations. **f** Normalized photoluminescence spectra of fresh CGF and **g** extracted PL bandgaps for 215 locations.

$l = 28$ (cm), validating the successful formation of all alloys on a single film. Raw absorption figures are shown in Supplementary Fig. 3.

Next, we measured photoluminescence (PL) of the CGF using the same optical probe (raw figures are shown in Supplementary Fig. 4). We then processed the data using MATLAB code (Supplementary Data 2) to normalize the PL spectra (Fig. 2f) and calculate the PL bandgaps (Fig. 2g). As expected, the PL bandgaps of the CGF follow the absorption bandgap trend (Fig. 2g, f).

Supplementary Fig. 4 shows raw PL data and extracted PL intensity and the full-width at half-maximum (FWHM) of the CGF. The bromide ($x < 0.15$) and iodide-dominant ($x > 0.7$) regions show excellent PL color purity with FWHM of <40 nm, while MAPb(I_xBr_{1-x})$_3$ alloys demonstrate significantly broad FWHM exceeding 50 nm, likely due to phase segregation[34,35,39]. The bromine-dominant perovskite region along the film shows strong PL peaks, in line with the recent findings of impressive green-emitting Br-rich perovskites[40].

We also performed micro-X-ray diffraction (mXRD) (Fig. 3b) to gain insights into the structural evolution of the CGF along the film. The first-order reflection of (001) planes has gradually shifted to lower diffraction angles (larger unit cell parameters), with the increase of l indicating of successful formation of solid MAPb(I_xBr_{1-x})$_3$ alloys along the film[41].

To quantify film heterogeneity across the width of the CGF, we measured the absorption, and PL bandgaps along 11 parallel lines

distanced 1 mm from one another using the robotic arm. We then normalized the bandgaps to the center of the CGF and show thus-obtained color maps in Fig. 2c. The figures demonstrate excellent homogeneity of the CGFs across the film (width); heterogeneity does not exceed ±8.5% and is mainly located at the edges of the film, likely due to the delayed exit of the ink from the sides of the slot-die head (positive heterogeneity values) or advanced release of ink due to roughness of the substrate (negative heterogeneity values).

The stability of halide perovskites is the subject of ongoing investigations. Compositional engineering, including I-Br alloying, has been an efficient method of addressing this issue. Taking advantage of all possible alloys on our CGF, we used it to study the stability of perovskite alloys. We aged the perovskite CGF at 30–40% relative humidity at room temperature, and regularly measured absorption, PL, and mXRD (Supplementary Figs. 3–5). To quantify the change by aging, we normalized the extracted values such as bandgap and lattice parameters of the aged film to those of fresh film (Supplementary Fig. 6) in the same location. In this representation, any inclination from 1 in the figures would indicate degradation. Figure 3a compares fresh CGF with the aged one, demonstrating a significant visual color change in most parts of the film, except in the Br-rich region at $x < 0.2$; this agrees with optical and structural characterization results that show Br-rich regions experience the lowest degree of degradation (Supplementary Fig. 6).
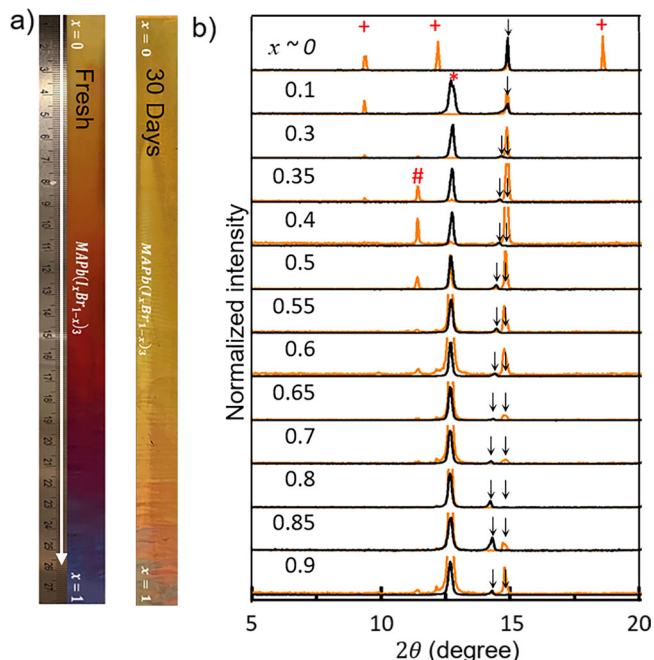
Fig. 3 Stability of MAPb(IxBr1-x)3 CGFs. a Photographs of fresh and aged CGF film. **b** mXRD spectra of fresh (black) and aged (orange) CGFs. The Bragg peaks assigned to perovskite (↓), PbI2 (*), MA4PbI6*2H2O (#), and MAPbBr3 and PbBr2 hydrates (+) are labeled.

Global inspection of mXRD spectra (Fig. 3b) indicates three degradation regimes in $MAPb(I_xBr_{1-x})_3$ alloys as a function of composition. In the Br-rich region with $x \leq 0.1$, degradation is mainly due to hydration and formation of hydrated $PbBr_2$ and $MAPbBr_3$ (corresponding changes are shown in Fig. 3b)[42,43]. In the iodide-rich region with $x \geq 0.9$, decomposition is mainly due to loss of the MAI and significant release of PbI_2 (a sharp increase of PbI_2 peak). In $MAPb(I_xBr_{1-x})_3$ alloys with $0.1 < x < 0.9$, degradation mostly occurs through segregation to Br-rich perovskite (shift of perovskite peak to higher diffraction angles in Fig. 3b) and $MA_4PbI_6*2H_2O$ and PbI_2[44]. This, to the best of our knowledge, is the first observation of multiple degradation modes in I-Br halide perovskite alloys[45].

Conclusion

In summary, we demonstrated a strategy for the fabrication of compositionally-graded films, a method that allows synthesizing all possible phases from binary systems in one shot. To exemplify the use of this method, we applied it to find stable regions in $MAPb(I_xBr_{1-x})_3$ compositions. This method can be used to search processing conditions and novel materials for batteries, catalysis, superconductors, and other fields, where compositional engineering plays a pivotal role. In Supplementary Fig. 7, we show $CuBr_xCl_{1-x}$ CGF, which can be used to optimize Cu catalyst for CO_2 electroreduction. The approach detailed in this work provides access to the gap-free database of binary materials enabling efficient and accurate machine-learning guided discovery of materials.

Methods

Materials and fabrication. MABr and MAI were purchased from Greatcell Solar. PbI_2, $PbBr_2$, and DMF were purchased from MilliporeSigma. All chemicals and solvents were used without any further modification. Perovskites inks were made by dissolving methylammonium halides CH_3NH_3X (X = Br or I) and PbX_2 in dimethylformamide (DMF) to prepare 1 M solutions.

Slot-die coating profile of CGFs is shown in Supplementary Fig. 1. Two solutions were placed in two Research Laboratory Coater (RLC) of infinityPV ApS

slot-die coater pumps. First, the dead volumes (from syringes till the end of the Y junction) were filled with inks at a speed of 0.05 ml/min, and then Y junction was attached to the slot-die head. Second, the slot-die head was filled with one ink until the ink appeared at the tip of the head at a speed of 0.24 ml/min. Third, the first ink supply is stopped, but the second ink is pumped at 0.3 ml/min speed simultaneously depositing the solution on the substrate. The mixed solution was deposited on a glass substrate placed on a hot plate with a fixed temperature of 140 °C. Supplementary Movie 1 shows the appearance of fabricated CGF.

Characterization. The gradient film measurements of all compositions were carried out via a UV-Vis AVENTES spectrometer (AvaSpec-ULS2048CL-EVO-RS) in the reflection mode. The absorption spectra of the gradient film were recorded in the wavelength range of 500–780 (nm) at the ambient temperature with an auto-saving option every 200 (ms) while moving the reflection probe through the gradient film. Using the same spectrometer in the reflection mode ranging from 500 to 780 nm, we measured the photoluminescence (PL) peaks in a dark room every 2 s. Dorna 2 robotic arm (Dorna robotics) was used to automate the process of acquisition of CGF's optical properties (Supplementary Movie 1). For mXRD measurement, PANalytical Empyrean system using a Cu source ($K_\alpha = 1.5406$ Å) was used. The data were collected in a high-throughput manner using a SAXS stage and PIXcel2D detector.

Data availability

The data sets generated during and/or analyzed during the current study are available from the corresponding author on reasonable request.

Code availability

The codes used in this study are attached as Supplementary Data 1 and Supplementary Data 2.

References

1. Lu, Z. Computational discovery of energy materials in the era of big data and machine learning: a critical review. *Mater. Reports Energy* **1**, 100047 (2021).
2. Xiao, K. et al. All-perovskite tandem solar cells with 24.2% certified efficiency and area over 1 cm² using surface-anchoring zwitterionic antioxidant. *Nat. Energy* **5**, 870–880 (2020).
3. Prashun, G., Vladan, S. & Eric, S. T. Computationally guided discovery of thermoelectric materials. *Nat. Rev. Mater.* **2**, 17053 (2017).
4. You, Y.-M. et al. An organic-inorganic perovskite ferroelectric with large piezoelectric response. *Science.* **357**, 306–309 (2017).
5. Liu, X. & Dai, L. Carbon-based metal-free catalysts. *Nat. Rev. Mater.* **1**, 16064 (2016).
6. Yuan, Y., Amine, K., Lu, J. & Shahbazian-Yassar, R. Understanding materials challenges for rechargeable ion batteries with in situ transmission electron microscopy. *Nat. Commun.* **8**, 15806 (2017).
7. Keimer, B., Kivelson, S. A., Norman, M. R., Uchida, S. & Zaanen, J. From quantum matter to high-temperature superconductivity in copper oxides. *Nat.* **518**, 179–186 (2015).
8. Spaldin, N. A. & Ramesh, R. Advances in magnetoelectric multiferroics. *Nat. Mater.* **18**, 203–212 (2019).
9. Ekins, S. et al. Exploiting machine learning for end-to-end drug discovery and development. *Nat. Mater.* **18**, 435–441 (2019).
10. Luo, X. & Xie, R. J. Recent progress on discovery of novel phosphors for solid state lighting. *J. Rare Earths* **38**, 464–473 (2020).
11. de Almeida, A. F., Moreira, R. & Rodrigues, T. Synthetic organic chemistry driven by artificial intelligence. *Nat. Rev. Chem.* **3**, 589–604 (2019).
12. Kauffman, G. B. & Mayo, I. The story of nitinol: the serendipitous discovery of the memory metal and its applications. *Chem. Educ.* **2**, 1–21 (1997).
13. Cui, M. et al. High-entropy metal sulfide nanoparticles promise high-performance oxygen evolution reaction. *Adv. Energy Mater.* **11**, 2002887 (2021).
14. Higgins, K., Valleti, S. M., Ziatdinov, M., Kalinin, S. V. & Ahmadi, M. Chemical robotics enabled exploration of stability in multicomponent lead halide perovskites via machine learning. *ACS Energy Lett.* **5**, 3426–3436 (2020).
15. Manion, J. G., Proppe, A. H., Hicks, G. E. J., Sargent, E. H. & Seferos, D. S. High-throughput screening of antisolvents for the deposition of high-quality perovskite thin films. *ACS Appl. Mater. Interfaces* **12**, 26026–26032 (2020).
16. Yang, W. et al. Balancing the efficiency, stability, and cost potential for organic solar cells via a new figure of merit. *Joule* **5**, 1209–1230 (2021).
17. Alstrup, J., Jørgensen, M., Medford, A. J. & Krebs, F. C. Ultra fast and parsimonious materials screening for polymer solar cells using differentially pumped slot-die coating. *ACS Appl. Mater. Interfaces* **2**, 2819–2827 (2010).

18. Sun, S. et al. Accelerated development of perovskite-inspired materials via high-throughput synthesis and machine-learning diagnosis. *Joule* **3**, 1437–1451 (2019).
19. Yoo, J. J. et al. Efficient perovskite solar cells via improved carrier management. *Nat.* **590**, 587–593 (2021).
20. Jiang, X. et al. One-step synthesis of $SnI_2 \cdot (DMSO)_x$ adducts for high-performance tin perovskite solar cells. *J. Am. Chem. Soc.* **143**, 10970–10976 (2021).
21. Dagar, J. et al. Compositional and interfacial engineering yield high-performance and stable p-i-n perovskite solar cells and mini-modules. *ACS Appl. Mater. Interfaces* **13**, 13022–13033 (2021).
22. Kalinin, S. V., Sumpter, B. G. & Archibald, R. K. Big–deep–smart data in imaging for guiding materials design. *Nat. Mater.* **14**, 973–980 (2015).
23. Alberi, K. et al. The 2019 materials by design roadmap. *J. Phys. D. Appl. Phys.* **52**, 013001 (2018).
24. Girolamo, D. D. I. et al. Solvents for processing stable tin halide perovskites. *ACS Energy Lett.* **6**, 959–968 (2021).
25. Ren, F. et al. Accelerated discovery of metallic glasses through iteration of machine learning and high-throughput experiments. *Sci. Adv.* **4**, eaaq156 (2018).
26. Li, J. et al. AI applications through the whole life cycle of material. *Discovery. Matter* **3**, 393–432 (2020).
27. Correa-Baena, J. P. et al. Accelerating materials development via automation, machine learning, and high-performance computing. *Joule* **2**, 1410–1420 (2018).
28. Brown, K. A., Brittman, S., Jariwala, D. & Celano, U. Machine learning in nanoscience: big data at small scales. *Nano Lett.* **19**, 30 (2021).
29. Jeon, N. J. et al. Compositional engineering of perovskite materials for high-performance solar cells. *Nature* **517**, 476–480 (2015).
30. Zhao, Y. et al. Discovery of temperature-induced stability reversal in perovskites using high-throughput robotic learning. *Nat. Commun.* **12**, 2191 (2021).
31. Cao, X. et al. Phase exploration and identification of multinary transition-metal selenides as high-efficiency oxygen evolution electrocatalysts through combinatorial electrodeposition. *ACS Catal.* **8**, 8273–8289 (2018).
32. Yang, Z. et al. Slot-die coating large-area formamidinium-cesium perovskite film for efficient and stable parallel solar module. *Sci. Adv.* **7**, 3749 (2021).
33. Choi, K. J., Lee, J. Y., Park, J. & Seo, Y. S. Multilayer slot-die coating of large-area organic light-emitting diodes. *Org. Electron.* **26**, 66–74 (2015).
34. Xiao, Z. et al. Mixed-halide perovskites with stabilized bandgaps. *Nano Lett.* **17**, 6863–6869 (2017).
35. Kundu, S. & Kelly, T. L. In situ studies of the degradation mechanisms of perovskite solar cells. *EcoMat* **2**, e12025 (2020).
36. Best Research-Cell Efficiency Chart | Photovoltaic Research | NREL (2022). https://www.nrel.gov/pv/cell-efficiency.html.
37. Sandström, A., Dam, H., Krebs, F. & Edman, L. Ambient fabrication of flexible and large-area organic light-emitting devices using slot-die coating. *Nat. Commun.* **3**, 1002 (2012).
38. Lee, C. Y., Chang, C. L., Wang, Y. N. & Fu, L. M. Microfluidic mixing: a review. *Int. J. Mol. Sci.* **12**, 3263–3287 (2011).
39. Mathew, P. S., DuBose, J. T., Cho, J. & Kamat, P. V. Spacer cations dictate photoinduced phase segregation in 2D mixed halide perovskites. *ACS Energy Lett.* **6**, 2499–2501 (2021).
40. Brennan, M. C., Ruth, A., Kamat, P. V. & Kuno, M. Photoinduced anion segregation in mixed halide perovskites. *Trends Chem.* **2**, 282–301 (2020).
41. Noh, J. H., Im, S. H., Heo, J. H., Mandal, T. N. & Seok, S. I. Chemical management for colorful, efficient, and stable inorganic-organic hybrid nanostructured solar cells. *Nano Lett.* **13**, 1764–1769 (2013).
42. Sharma, S. K. et al. Reversible dimensionality tuning of hybrid perovskites with humidity: visualization and application to stable solar cells. *Chem. Mater.* **31**, 3111–3117 (2019).
43. Ahmad, Z. & Mishra, A. Growth of $PbBr_2$ microrods with unique structure and surface morphology. *J. Mater. Sci. Mater. Electron.* **31**, 4672–4676 (2020).
44. Leguy, A. M. A. et al. Reversible hydration of $CH_3NH_3PbI_3$ in films, single crystals, and solar cells. *Chem. Mater.* **27**, 3397–3407 (2015).
45. Ruess, R., Benfer, F., Böcher, F., Stumpp, M. & Schlettwein, D. Stabilization of organic–inorganic perovskite layers by partial substitution of iodide by bromide in methylammonium lead iodide. *ChemPhysChem* **17**, 1505–1511 (2016).

Author contributions

S.M. and S.K. developed the gradient fabrication method via slot-die coating. S.M. prepared the films for measurements, collected, and analyzed absorption and PL data, set the robotic configurations to automate the measurements, wrote the codes with MATLAB for processing the data. S.K. and V.Y. collected the pXRD data and helped with the analysis. O.V. and M.R. assisted with evaluating measurement outcomes. S.M., SK., and M.I.S. co-wrote the manuscript. M.I.S. supervised the project. All authors provided feedback on the manuscript.

Competing interests

The authors declare no competing interests.

Additional information

Supplementary information The online version contains supplementary material available at https://doi.org/10.1038/s43246-022-00235-5.

Correspondence and requests for materials should be addressed to Makhsud I. Saidaminov.

Peer review information *Communications Materials* thanks Eva Unger and the other, anonymous, reviewer for their contribution to the peer review of this work. Primary Handling Editor: John Plummer. Peer reviewer reports are available.

Reprints and permission information is available at http://www.nature.com/reprints

Publisher's note Springer Nature remains neutral with regard to jurisdictional claims in published maps and institutional affiliations.